Frequency Domain Analysis of Dual Active Bridge Converter Considering All Power Losses Elements

Seyed Omid Golpayegani[1], Mostafa Jazaeri[1*], Naser Eskandarian[1]

Abstract—**Modeling of power electronic converters plays a significant role in examining the behaviour and designing control systems. Dual Active Bridge (DAB) converters, due to many advantages such as inherent soft-switching, bidirectional power transfer, and higher energy density, are used in various applications such as SST transformers, smart grids, and electric vehicle battery chargers. In this paper, a new reduced-order model for a DAB converter is introduced by modeling nonlinear elements such as semiconductor devices and transformers. By considering all power loss elements, and input/output filters, the modeling becomes more realistic. The performance and accuracy of the proposed model is improved compared to conventional reduced-order methods. Small signal modeling for the DAB converter is curried out and control transfer functions of the system are investigated. Additionally, frequency response analysis of the proposed model under different conditions is compared with the detailed model of the DAB converter containing nonlinear elements implemented in PLECS software. Simulation results demonstrate a satisfactory accuracy of the proposed model in assessing the performance and dynamic behavior of the DAB converter under various operating conditions.**

Index Terms—**DAB, Reduced Order Model, Small Signal Modeling, Frequency Response Analysis.**

I. INTRODUCTION

AMOUNG PWM converters, the Dual Active Bridge converters (DAB) [1], with their inherent advantages including a lower number of passive elements, higher power density, greater energy efficiency, and galvanic isolation, as well as the capability for bi-directional power transfer, has emerged as one of the most widely adopted converter technologies in various applications. These applications include Solid-State Transformers (SST) [2], Smart-Grid Applications [3]-[5] and Battery Chargers for electric and hybrid electric vehicles [6-9]. In [10],[11], a complete overview and comparison of modulation and control strategies, the soft-switching strategy, efficiency improvement strategy, design considerations, and dynamic response optimization for DAB DC-DC converters have been widely studied.The required energy is provided by the leakage inductance of the transformer. Creating a resonance circuit between the leakage inductance and the output capacitors of one leg switches in a full bridge converter leads to charging and discharging the output capacitance of each switch before its

corresponding switch transitions. Therefore, each switch's output capacitance is fully discharged before its corresponding switch turns on. In [12], triple phase-shift modulation (TPS) is proposed. It is a generalized form of phase-shift control, of which SPS, DPS and EPS are special cases. TPS control can achieve minimum current stress, minimum power loss, maximum efficiency, and the maximum Zero Voltage Switching (ZVS) range among all modulation methods. Therefore, the performance of a DAB converter with TPS control mode has the most practical application.

Modeling plays an important part in power electronic circuit analysis. Clear analysis of physical data is made possible by converter models. However, when using classical control theory to examine nonlinear systems, such as power electronic circuits, it is typically necessary to build a large-signal model first, then linearize it to create a small-signal model for additional examination. There are now four main methods for simulating DAB converters. The reduced-order modeling method is extensively utilized in DAB-related research due to its straightforwardness and precise illustration of the DAB converter's operational process. Furthermore, the remaining three methods called state-space averaging, generalized state-space averaging, and discrete-time modeling are also employed in the design of DAB controllers. By eliminating dynamics from transformer inductor current in DAB, a reduced order model is built [13]-[15]. The generalized state-space averaging technique is introduced to mitigate the constraints of the conventional state-space averaging method in explaining the fluctuations in AC quantities [16]. The generalized state-space averaging modeling approach for the DAB converter is utilized in [17]. A discrete-time modeling methodology also has the capability to understand the high-frequency dynamic phenomena of DAB and has been extensively employed in the modeling of power converters [18]-[20]. In discrete-time modeling, the discrete state equations are derived by sampling the DAB at various time intervals, resulting in modifications to the coefficient matrix of the differential equations in the state equation [21]. Each of the above modeling methods has better accuracy in specific applications. In the instance of the generalized state-space averaging method, although a full-order model theoretically is expected to attain superior accuracy, this accuracy might be undermined in the presence of significant harmonic distortions, as the full-order model relies only on the first harmonic [22]. Discrete-time modeling methods offer enhanced modeling precision, particularly beneficial for

---

analyzing the dynamic behavior of systems and designing control strategies. In terms of modeling precision, reduced-order modeling is a strategy employed to modify complicated system models. It accomplishes this by eliminating specific high-level dynamics or nonlinear features of the system, thereby decreasing the model to a lower-level one. While the DAB is streamlined to a lower-level model, it does not undermine the accuracy of the model, as this is identified by the inherent attributes of the DAB topology [23]. The comparative results between various modeling methods and the detailed model demonstrate that the reduced-order modeling technique showcases the adequate precision compared to the actual model [24]. In recent years, extensive research has been conducted on reduced-order modeling for DAB converters [25]-[27]. Moreover, reduced-order models for DAB converters are also recognized as average value models (AVM). Dependent current sources are used instead of switching elements in converter modeling. The values of these dependent current sources are equivalent to the average current passing through the converter's switching elements. The lossless AVM for DAB is obtained in [28] using the conventional state-space averaging method [29]. Subsequently, the output current is calculated for the ideal scenario. However, excluding elements contributing to system losses from the model diminishes its overall effectiveness. In [30], the effects of transformer core losses and DAB semiconductor conduction loss are examined in relation to the SPS modulation method. Reduced-order average value model (RAVM) research and consideration of the effects of transformer core losses and converter switching conduction losses in the DAB converter for TPS modulation are presented in [31]. However, modeling accuracy is compromised, especially at higher frequencies, when switching power losses are ignored when derived from the reduced-order model for the DAB converter. In order to improve the accuracy of steady state and dynamic response prediction, particularly for high frequency applications, this work provides a new RAVM for a DAB converter that takes into account all parasitic elements and switching power loss virtual resistors (RSW).

Section II focuses on introducing a detailed model of the DAB converter suitable for electric vehicle charger applications, alongside the TPS modulation method and soft-switching conditions. Additionally, it discusses the use of state-space equations and derives the switching loss function for both large and small signal models. Section III presents the small-signal model of the DAB converter. Section IV details the extraction of control transfer functions using the small-signal model and discusses the frequency response of the DAB converter under different operating conditions, verifying through simulation. Section V concludes the article.

II. DAB DETAILED MODEL SUITABLE FOR ELECTRIC CAR CHARGER APPLICATIONS

The schematic of a bidirectional DAB, depicting all circuit elements connected to the DC link, is illustrated in Fig. 1. This converter comprises an input LC filter, a high-frequency transformer (with a ratio of 1:n), two active bridge converters—one on the primary side and the other on the secondary side of the transformer—an LC output filter, and an output load. The high-frequency transformer provides galvanic isolation and facilitates energy transfer through its winding. Moreover, RC

branches are incorporated into LC filters to mitigate voltage and current ripples. The input/output filters are considered as an LC structure with an RC damping branch designed to eliminate current and voltage ripples. The switching turn-on resistors Rs, switch capacitors Cs, winding resistors Rl1 and Rl2, leakage inductors Ll1 and Ll2, equivalent core loss resistance RM, transformer magnetizing inductor LM are included.

To examine the effect of parasitic elements on the dynamic response of the converter, switching devices on both the main and secondary sides are taken into consideration as diodes and capacitance. The thorough model includes transformer losses, inductor losses, switching losses, and conduction loss to improve modeling accuracy. It is important to remember that adding parasitic capacitance to the model makes it more accurate, particularly when frequencies are high. In this article, a virtual resistor that is suggested to simulate switching losses in the DAB converter is introduced.
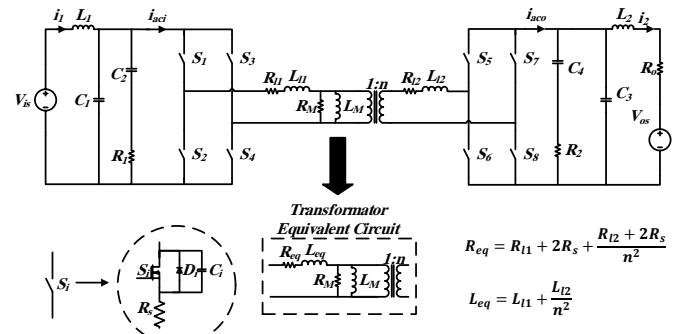

Fig. 1. Bidirectional DAB Detailed Model

A. DAB Modulation Techniques

Basic characterization, operating points, and modulation strategies for the DAB converter are discussed in [11]. While SPS modulation is the simplest, it has limitations in the voltage transmission ratio and transmission power. To address these constraints, DPS and EPS modulation modes are proposed. However, as DPS modulation and EPS modulation are special forms of TPS modulation, as mentioned in [11], the model of DAB with TPS modulation strategy has more practical aspects. Therefore, TPS has been selected in this paper to derive a general model for all modulation schemes.

B. DAB Operation Modes

The DAB converter employs a triple-shift modulation and has four operational modes in each half cycle as shown in Fig. 2. Its operation in the second half cycle is similar to the first half cycle.

Stage 1 ($t_0 \leq t < t_1$): during this time interval, pair switches (S_1,S_3) and (S_6,S_7) are in one state. At time t_1, S_3 turning off and S_4 turning on. The current goes through switches is equal to I_{t1}.

Stage 2 ($t_1 \leq t < t_2$): during this time interval, pair switches (S_1,S_4) and (S_6,S_7) are inone state. At t_2 transition, S_6 turning off and S_5 turning on. At this moment, the switching current on the secondary side equals the sum of the leakage inductor current, transformer magnetizing inductor current and transformer resistance current, all referred to the secondary side.

Stage 3 ($t_2 \leq t < t_3$): during this time interval, pair switches (S_1,S_4) and (S_5,S_7) are in one state. At t_3 transition, S_7 turning off and S_8 turning on. At this moment, the switching current on

the secondary side equals the sum of the leakage inductor current and transformer magnetizing inductor current referred to the secondary side.

Stage 4 ($t_3 \leq t < t_4$): during this time interval, pair switches (S_1,S_4) and (S_5,S_8) are in on state. At t_3 transition, S_1 turning off and S_2 turning on. The current at t_4 transition is equal to I_{t4}.
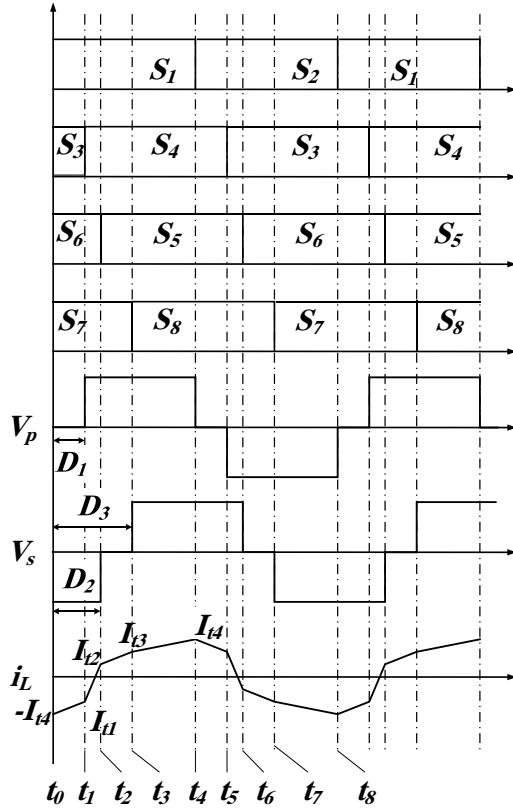

Fig. 2. DAB Main operation Waveforms with TPS modulation

C. DAB Steady-Space Equations

In order to obtain the large-signal model of the DAB converter, steady-state equations are used. Input and output currents (i_{aci}, i_{aco}) have periodic changes as shown in Fig. 2. Then, by averaging over one cycle, the average value large-signal model of the DAB converter can be obtained. The schematic of the DAB converter along with the steady-space equations is shown in Fig. 3.
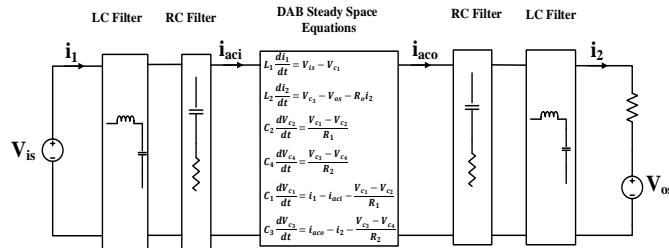

Fig. 3. DAB Steady-Space Schematic

Finally, average currents ($\bar{I}_{aci}$, $\bar{I}_{aco}$) can be obtained during the period T as follows

$$
\begin{aligned}
\bar{I}_{aci} = {} & \frac{V_{c_1} + V'_{c_3}}{R_{eq}}(D_2 - D_1) + \frac{V_{c_1}}{R_{eq}}(D_3 - D_2) - \frac{V_{c_1} - V'_{c_3}}{R_{eq}}(1 - D_3) \\
& - \frac{1}{T} \times \frac{L_{eq}}{R_{eq}} \times \left(I_{t_1} - \frac{V_{c_1} + V'_{c_3}}{R_{eq}}\right) \times \left(e^{-\frac{R_{eq}}{L_{eq}}(D_2 - D_1)T} - 1\right) \\
& - \frac{1}{T} \times \frac{L_{eq}}{R_{eq}} \times \left(I_{t_2} - \frac{V_{c_1}}{R_{eq}}\right) \times \left(e^{-\frac{R_{eq}}{L_{eq}}(D_3 - D_2)T} - 1\right) \\
& - \frac{1}{T} \times \frac{L_{eq}}{R_{eq}} \times \left(I_{t_3} - \frac{V_{c_1} - V'_{c_3}}{R_{eq}}\right) \times \left(e^{-\frac{R_{eq}}{L_{eq}}(1 - D_3)T} - 1\right)
\end{aligned}
\tag{1}
$$

$$
\begin{aligned}
n \times \bar{I}_{aco} = {} & -\frac{V'_{c_3}}{R_{eq}}D_1 - \frac{V_{c_1} + V'_{c_3}}{R_{eq}}(D_2 - D_1) + \frac{V_{c_1} - V'_{c_3}}{R_{eq}}(1 - D_3) \\
& - \frac{1}{T} \times \frac{L_{eq}}{R_{eq}} \times \left(I_{t_4} + \frac{V'_{c_3}}{R_{eq}}\right) \times \left(e^{-\frac{R_{eq}}{L_{eq}}D_1 T} - 1\right) \\
& + \frac{1}{T} \times \frac{L_{eq}}{R_{eq}} \times \left(I_{t_1} - \frac{V_{c_1} + V'_{c_3}}{R_{eq}}\right) \times \left(e^{-\frac{R_{eq}}{L_{eq}}(D_2 - D_1)T} - 1\right) \\
& - \frac{1}{T} \times \frac{L_{eq}}{R_{eq}} \times \left(I_{t_3} - \frac{V_{c_1} - V'_{c_3}}{R_{eq}}\right) \times \left(e^{-\frac{R_{eq}}{L_{eq}}(1 - D_3)T} - 1\right) - \frac{V'_{c_3}}{R_M} - \frac{V'_{c_3}}{R_{SW}}
\end{aligned}
\tag{2}
$$

Energy charge and discharge intervals in L_M during one cycle, with a period of 2T, are equal. In other words, the average magnetizing current becomes zero. Consequently, the average output current ($\bar{I}_{aco}$) considering the influence of the magnetic core resistance (R_M) in equation 14, becomes evident. Moreover, it also demonstrates the impact of considering a virtual resistance for the switching power losses (R_{sw}). Following sections address the method of calculating the switching power losses and determining the proposed virtual resistance value (R_{sw}) in this article.

D. Switching Loss Estimation

By considering the average input and output currents of the DAB converter ($\bar{I}_{aci}$, $\bar{I}_{aco}$) using equations (1) and (2), the impact of switch conduction losses is observed in these equations. Consequently, the impact of switching power losses on the suggested DAB converter model is discussed in this section. Two full-bridge (FB) converters make up a DAB converter. As a result, the DAB converter's switching power losses are equivalent to the sum of the losses from eight switches. Only the switching power loss during turn-off is taken into account, as the switches only function in ZVS mode when turned on. The detailed calculations for MOSFET power losses are given in [32], where equation (3) specifies the turn-off switching power losses for all switches in the DAB converter.

$$
P_{SW} = \sum_{i=1}^{8} \frac{1}{2} V_{sw_i} I_{sw_i}(t_{on} + t_{off}) f_{sw}
\tag{3}
$$

The DAB converter operates under ZVS turn-on conditions with TPS modulation. In Fig. 2, switches (S_1, S_3) and (S_6, S_7) are assumed to be turned on at time t_0. At time t_1, a resonant circuit is formed by the output capacitors of switches (S_3, S_4) and the leakage inductor of the transformer. This ensures that before switch $S4$ is turned on, its output capacitor is fully discharged. Consequently, ZVS turn-on performance is inherently considered under TPS modulation conditions. Therefore, the total switching loss can be calculated by (4) for total switching turn-off losses.

$$P_{SW} = \frac{1}{2}V_{c_1}\left(I_{t_1} + I_{t_4}\right) \times \left(t_{on} + t_{off}\right)f_{sw} \times 2$$
$$+ \frac{1}{2}V'_{c_3}\left(I_{t_2} - I_{t_3} + \frac{V'_{c_3}}{R_M}\right) \times \left(t_{on} + t_{off}\right)f_{sw} \times 2 \qquad (4)$$

To understand the effect of power losses on converter modeling, the following simplifications are considered. First, L_M and R_M are much larger than R_{eq} and L_{eq}, the effect on switching power loss can be ignored. As another assumption, the DAB voltage gain (V_{is}/V_{os}) is approximately equal to $1/n$ for optimal operating situations. Therefore, it is assumed the following equation holds in the steady state.

$$\frac{V_{c_1}}{V_{c_3}} \cong \frac{1}{n} \qquad (5)$$

By these assumptions, (4) can be formulated as

$$P_{SW} = V_{c_1}\left(I_{t_1} + I_{t_4} + I_{t_2} - I_{t_3}\right) \times \left(t_{on} + t_{off}\right)f_{sw} \qquad (6)$$

As shown in Fig. 2, the current i_L is piecewise linear. Therefore, the following relations can be inferred

$$L_{eq}\frac{\left(I_{t_1} + I_{t_4}\right)}{d_1 T} = V'_{c_3} \qquad (7)$$

$$L_{eq}\frac{\left(I_{t_3} - I_{t_2}\right)}{(d_3 - d_2)T} = V_{c_1} \qquad (8)$$

Finally, by substituting (7), (8) into (6) a simplified switching power loss can be obtained as

$$P_{SW} = \frac{V_{c_1}^2}{2L_{eq}}(d_1 + d_2 - d_3) \times \left(t_{on} + t_{off}\right)f_{sw} \qquad (9)$$

According to simplified switching power loss equation, the virtual switching resistance can be derived as follow:

$$R_{SW} = \frac{V_{c_1}^2}{P_{SW}} = \frac{2L_{eq}}{(d_1 + d_2 - d_3)\left(t_{on} + t_{off}\right)} \qquad (10)$$

E. Proposed RAVM for DAB Converter

By considering the average input and output currents according to equations (1) and (2), nonlinear elements like semiconductor devices and transformers can be represented as two dependent current sources. Thus, integrating switching power loss as R_{sw} results in a new Reduced Average Value Model (RAVM), depicted in Fig. 4. Given that the switching elements have been eliminated in this model, its implementation in the simulation will be much faster than the detailed model. Small signal analysis and control transfer functions are also achievable.
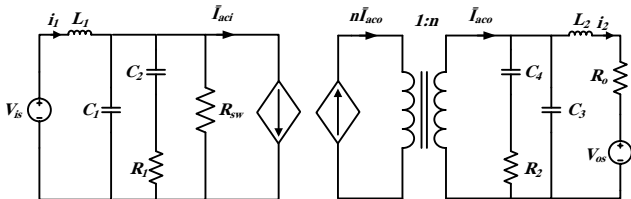

Fig. 4. DAB RAVM considering all lossy elements

III. SMALL SIGNAL MODEL OF DAB

To construct a small signal model for DAB converter around a DC operating point, the parameters must be considered as the sum of two components of a constant DC value and a small ac distortion value. The small-signal model for the DAB converter can be obtained similarly to the large-signal model as Fig. 5. The only difference lies in the values of the input and output currents ($\hat{I}_{aci}$, $\hat{I}_{aco}$) specified in Fig. 5.

$$\hat{I}_{aci} = p_1\hat{d}_1 + p_2\hat{d}_2 + p_3\hat{d}_3 + q\hat{v}_{c_1} + r\hat{v}_{c_3}$$
$$n\hat{I}_{aco} = x_1\hat{d}_1 + x_2\hat{d}_2 + x_3\hat{d}_3 + y\hat{v}_{c_1} + z\hat{v}_{c_3}$$
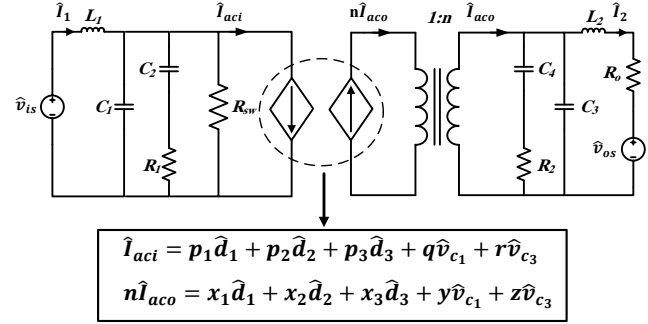
Fig. 5. DAB Small Signal RAVM considering all lossy elements

The small-signal model for the DAB converter can be obtained from equation (11)-(18) as follows:

$$L_1\frac{d\hat{i}_1}{dt} = \hat{v}_{is} - \hat{v}_{c_1} \qquad (11)$$

$$L_2\frac{d\hat{i}_2}{dt} = \hat{v}_{c_3} - \hat{v}_{os} - R_o\hat{i}_2 \qquad (12)$$

$$C_2\frac{d\hat{v}_{c_2}}{dt} = \frac{\hat{v}_{c_1} - \hat{v}_{c_2}}{R_1} \qquad (13)$$

$$C_4\frac{d\hat{v}_{c_4}}{dt} = \frac{\hat{v}_{c_3} - \hat{v}_{c_4}}{R_2} \qquad (14)$$

$$C_1\frac{d\hat{v}_{c_1}}{dt} = \hat{i}_1 - \hat{i}_{aci} - \frac{\hat{v}_{c_1} - \hat{v}_{c_2}}{R_1} - \frac{\hat{v}_{c_1}}{R_{SW}} \qquad (15)$$

$$C_3\frac{d\hat{v}_{c_3}}{dt} = \hat{i}_{aco} - \hat{i}_2 - \frac{\hat{v}_{c_3} - \hat{v}_{c_4}}{R_2} \qquad (16)$$

$$\hat{i}_{aci} = p_1\hat{d}_1 + p_2\hat{d}_2 + p_3\hat{d}_3 + q\hat{v}_{c_1} + r\hat{v}_{c_3} \qquad (17)$$

$$n \times \hat{i}_{aco} = x_1\hat{d}_1 + x_2\hat{d}_2 + x_3\hat{d}_3 + y\hat{v}_{c_1} + z\hat{v}_{c_3} \qquad (18)$$

Where, the coefficients specified in equations (17) and (18) are as follows:

$$p_1 = -\frac{V_{c_1} + V'_{c_3}}{R_{eq}} + \frac{V_{c_1}e^{-\frac{R_{eq}D_1T}{L_{eq}}} + V_{c_1}e^{-\frac{R_{eq}(1-D_1)T}{L_{eq}}}}{R_{eq}\left(1 + e^{-\frac{R_{eq}}{L_{eq}}T}\right)}$$
$$+ \frac{V'_{c_3}e^{-\frac{R_{eq}(1+D_1-D_2)T}{L_{eq}}} + V'_{c_3}e^{-\frac{R_{eq}(1+D_1-D_3)T}{L_{eq}}}}{R_{eq}\left(1 + e^{-\frac{R_{eq}}{L_{eq}}T}\right)} \qquad (19)$$

$$p_2 = \frac{V'_{c_3}}{R_{eq}} - \frac{V'_{c_3}e^{-\frac{R_{eq}(1-D_2)T}{L_{eq}}} + V'_{c_3}e^{-\frac{R_{eq}(1+D_1-D_2)T}{L_{eq}}}}{R_{eq}\left(1 + e^{-\frac{R_{eq}}{L_{eq}}T}\right)} \qquad (20)$$

$$p_3 = \frac{V'_{c_3}}{R_{eq}} - \frac{V'_{c_3}e^{-\frac{R_{eq}(1-D_3)T}{L_{eq}}} + V'_{c_3}e^{-\frac{R_{eq}(1+D_1-D_3)T}{L_{eq}}}}{R_{eq}\left(1 + e^{-\frac{R_{eq}}{L_{eq}}T}\right)} \qquad (21)$$

$$q = \frac{1 - D_1}{R_{eq}}$$

$$-\frac{1}{T} \times \frac{L_{eq}}{R_{eq}} \times \frac{1 + e^{-\frac{R_{eq}}{L_{eq}}D_1 T} - e^{-\frac{R_{eq}}{L_{eq}}(1-D_1)T} - e^{-\frac{R_{eq}}{L_{eq}}T}}{R_{eq}\left(1 + e^{-\frac{R_{eq}}{L_{eq}}T}\right)} \tag{22}$$

$$r = \frac{1}{n}$$

$$\left[\begin{array}{c} -\frac{1 + D_1 - D_2 - D_3}{R_{eq}} + \frac{1}{T} \times \frac{L_{eq}}{R_{eq}} \times \frac{2 - e^{-\frac{R_{eq}}{L_{eq}}(1-D_2)T} - e^{-\frac{R_{eq}}{L_{eq}}(1-D_3)T}}{R_{eq}\left(1 + e^{-\frac{R_{eq}}{L_{eq}}T}\right)} \\ -\frac{1}{T} \times \frac{L_{eq}}{R_{eq}} \times \frac{e^{-\frac{R_{eq}}{L_{eq}}(1+D_1-D_2)T} + e^{-\frac{R_{eq}}{L_{eq}}(1+D_1-D_3)T} - 2e^{-\frac{R_{eq}}{L_{eq}}T}}{R_{eq}\left(1 + e^{-\frac{R_{eq}}{L_{eq}}T}\right)} \end{array}\right] \tag{23}$$

$$x_1 = \frac{V_{c_1}}{R_{eq}} - \frac{V_{c_1}e^{-\frac{R_{eq}}{L_{eq}}(D_2-D_1)T} + V_{c_1}e^{-\frac{R_{eq}}{L_{eq}}(D_3-D_1)T}}{R_{eq}\left(1 + e^{-\frac{R_{eq}}{L_{eq}}T}\right)} \tag{24}$$

$$x_2 = -\frac{V_{c_1} + V'_{c_3}}{R_{eq}} + \frac{V_{c_1}e^{-\frac{R_{eq}}{L_{eq}}D_2 T} + V_{c_1}e^{-\frac{R_{eq}}{L_{eq}}(D_2-D_1)T}}{R_{eq}\left(1 + e^{-\frac{R_{eq}}{L_{eq}}T}\right)}$$

$$+ \frac{V'_{c_3}e^{-\frac{R_{eq}}{L_{eq}}(D_3-D_2)T} + V'_{c_3}e^{-\frac{R_{eq}}{L_{eq}}(1+D_2-D_3)T}}{R_{eq}\left(1 + e^{-\frac{R_{eq}}{L_{eq}}T}\right)} \tag{25}$$

$$x_3 = -\frac{V_{c_1} - V'_{c_3}}{R_{eq}} + \frac{V_{c_1}e^{-\frac{R_{eq}}{L_{eq}}D_3 T} + V_{c_1}e^{-\frac{R_{eq}}{L_{eq}}(D_3-D_1)T}}{R_{eq}\left(1 + e^{-\frac{R_{eq}}{L_{eq}}T}\right)}$$

$$- \frac{V'_{c_3}e^{-\frac{R_{eq}}{L_{eq}}(D_3-D_2)T} + V'_{c_3}e^{-\frac{R_{eq}}{L_{eq}}(1+D_2-D_3)T}}{R_{eq}\left(1 + e^{-\frac{R_{eq}}{L_{eq}}T}\right)} \tag{26}$$

$$y = \frac{1 + D_1 - D_2 - D_3}{R_{eq}} + \frac{1}{T} \times \frac{L_{eq}}{R_{eq}} \times \frac{2 - e^{-\frac{R_{eq}}{L_{eq}}D_2 T} - e^{-\frac{R_{eq}}{L_{eq}}D_3 T}}{R_{eq}\left(1 + e^{-\frac{R_{eq}}{L_{eq}}T}\right)}$$

$$-\frac{1}{T} \times \frac{L_{eq}}{R_{eq}} \times \frac{e^{-\frac{R_{eq}}{L_{eq}}(D_2-D_1)T} + e^{-\frac{R_{eq}}{L_{eq}}(D_3-D_1)T} - 2e^{-\frac{R_{eq}}{L_{eq}}T}}{R_{eq}\left(1 + e^{-\frac{R_{eq}}{L_{eq}}T}\right)} \tag{27}$$

$$z = \frac{1}{n}\left[\begin{array}{c} \frac{1}{T} \times \frac{L_{eq}}{R_{eq}} \times \frac{1 - e^{-\frac{R_{eq}}{L_{eq}}(1+D_2-D_3)T} + e^{-\frac{R_{eq}}{L_{eq}}(D_3-D_2)T} - e^{-\frac{R_{eq}}{L_{eq}}T}}{R_{eq}\left(1 + e^{-\frac{R_{eq}}{L_{eq}}T}\right)} \\ -\frac{1 + D_2 - D_3}{R_{eq}} - \frac{1}{R_{SW}} - \frac{1}{R_M} \end{array}\right] \tag{28}$$

IV. FREQUENCY DOMAIN ANALYSIS

In Section III, the small-signal modeling of the DAB converter is addressed by linearizing the nonlinear differential steady-state equations of the system (Equations 30-37). By deriving control-to-output and control-to-input transfer functions, an analysis of the converter in the frequency domain can be conducted, enabling the study of the impact of each control parameter on the converter's performance. In calculating the transfer functions of the DAB converter, the control variables are the phase shift ratios (D_1, D_2, D_3). Additionally, the input parameter is assumed to be the input

source current (i_1), and the output parameter is equivalent to the load current (i_2). Using the Laplace transform to solve the differential steady-state equations of the system, control-to-output transfer functions and control-to-input transfer functions can be obtained. Therefore, the control-to-output transfer function and the output current of the DAB converter can be derived as equations (29) to (34).

$$I_2(s) = G_{od_1}(s)d_1(s) + G_{od_2}(s)d_2(s) + G_{od_3}(s)d_3(s) \tag{29}$$

$$G_{od_1}(s) = \frac{\hat{\imath}_2(s)}{\hat{d}_1(s)}\Big|_{\hat{d}_2(s)=\hat{d}_3(s)=\hat{v}_{in}(s)=\hat{v}_{os}(s)=0}$$

$$= \frac{1}{R_o + L_2 s} \times \frac{x_1 - yp_1/G_{A_1}(s)}{nG_{A_2}(s) + yr/G_{A_1}(s)} \tag{30}$$

$$G_{od_2}(s) = \frac{\hat{\imath}_2(s)}{\hat{d}_2(s)}\Big|_{\hat{d}_1(s)=\hat{d}_3(s)=\hat{v}_{in}(s)=\hat{v}_{os}(s)=0}$$

$$= \frac{1}{R_o + L_2 s} \times \frac{x_2 - yp_2/G_{A_1}(S)}{nG_{A_2}(s) + yr/G_{A_1}(s)} \tag{31}$$

$$G_{od_3}(s) = \frac{\hat{\imath}_2(s)}{\hat{d}_3(s)}\Big|_{\hat{d}_1(s)=\hat{d}_2(s)=\hat{v}_{in}(s)=\hat{v}_{os}(s)=0}$$

$$= \frac{1}{R_o + L_2 s} \times \frac{x_3 - yp_3/G_{A_1}(s)}{nG_{A_2}(s) + yr/G_{A_1}(s)} \tag{32}$$

$$G_{A_1}(s) = \left(\frac{1}{R_1} + C_1 s + q + \frac{1}{L_1 s} - \frac{1/R_1}{1 + R_1 C_2 s}\right) \tag{33}$$

$$G_{A_2}(s) = \left(\frac{1}{R_2} + C_3 s - \frac{z}{n} + \frac{1}{R_o + L_2 s} - \frac{1/R_2}{1 + R_2 C_4 s}\right) \tag{34}$$

Similarly, the input current and the control-to-input transfer function are represented in equations (35) to (38).

$$I_1(s) = G_{id_1}(s)d_1(s) + G_{id_2}(s)d_2(s) + G_{id_3}(s)d_3(s) \tag{35}$$

$$G_{id_1}(s) = \frac{\hat{\imath}_1(s)}{\hat{d}_1(s)}\Big|_{\hat{d}_2(s)=\hat{d}_3(s)=\hat{v}_{in}(s)=\hat{v}_{os}(s)=0}$$

$$= \frac{1}{L_1 s} \times \frac{np_1 + rx_1/G_{A_2}(s)}{nG_{A_1}(s) + yr/G_{A_2}(s)} \tag{36}$$

$$G_{id_2}(s) = \frac{\hat{\imath}_1(s)}{\hat{d}_2(s)}\Big|_{\hat{d}_1(s)=\hat{d}_3(s)=\hat{v}_{in}(s)=\hat{v}_{os}(s)=0}$$

$$= \frac{1}{L_1 s} \times \frac{np_2 + rx_2/G_{A_2}(s)}{nG_{A_1}(s) + yr/G_{A_2}(s)} \tag{37}$$

$$G_{id_3}(s) = \frac{\hat{\imath}_1(s)}{\hat{d}_3(s)}\Big|_{\hat{d}_1(s)=\hat{d}_2(s)=\hat{v}_{in}(s)=\hat{v}_{os}(s)=0}$$

$$= \frac{1}{L_1 s} \times \frac{np_3 + rx_3/G_{A_2}(s)}{nG_{A_1}(s) + yr/G_{A_2}(s)} \tag{38}$$

The frequency domain analysis of the converter in the steady-state operating points with d_1=0.2, d_2=0.5 and d_3=0.7 are obtained and the results are examined by each of the following conditions.

1) d_1 as sum of DC and small signal perturbation, d_2=0.5 and d_3=0.7

2) d_2 as sum of DC and small signal perturbation, $d_1=0.2$ and $d_3-d_2=0.2$

3) d_3 as sum of DC and small signal perturbation, $d_1=0.2$ and $d_2=0.5$

In this analysis, a small signal disturbance is added to DC operating point of phase shift ratios as below. Therefore, the actual phase shift ratio become a function of time, i.e.:

$$d_1(t) = D_1 + A_{m_1} \sin(2\pi f_{p_1 t}) \tag{39}$$

$$d_2(t) = D_2 + A_{m_2} \sin(2\pi f_{p_2 t}) \tag{40}$$

$$d_3(t) = D_3 + A_{m_3} \sin(2\pi f_{p_3 t}) \tag{41}$$

Where $A_{m1}=A_{m2}=A_{m3}=0.02$ is the amplitude and f_p ranging from 40 Hz to 6.25 kHz is the frequency of perturbation. The comparison of bode plots derived from detailed model and the proposed model are shown in Fig. 6-9 for 4 different cases as described later.

A. Case 1: Phase Shift Modulation $(D_1 = 0 \cdot 0 < D_2 < 1 \cdot D_3 - D_2 = 0)$

This situation is similar to SPS modulation. It is assumed that the value of D_1 is zero and the phase-shift ratios D_2 and D_3 change together. Bode diagram for this case is depicted in Fig. 6. As it can be seen, the proposed model closely captures the behavioral characteristics of the DAB converter circuit detailed model.
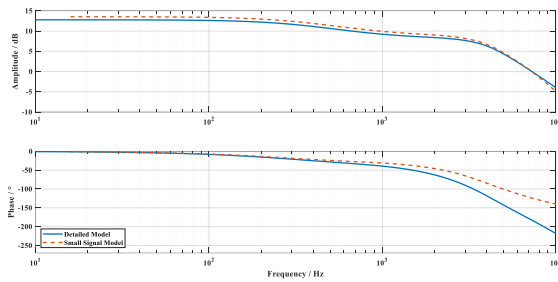

Fig. 6. Comparison detailed model and the proposed model for case 1.

B. Case 2: Duty Ratio Modulation for Primary Bridge $(0 < D_1 < D_2 < 1 \cdot D_3 - D_2 = 0)$

This situation is similar to EPS modulation. In this state, the phase-shift ratios D_2 and D_3 are equal, and there is no delay between pair switches (S_5,S_8) and (S_6,S_7) in the secondary bridge. Only the secondary bridge has a phase shift relative to the primary bridge. In the primary bridge diagonal switches (S_1,S_4) and (S_2,S_3) have the inner phase shift D_1 relative to each other. The phase-shift ratio of the primary side transformer bridge (D_1) is variable and has a value greater than zero and less than the constant phase-shift ratio of the secondary side transformer bridge. Bode diagram in this case is depicted in Fig. 7. As seen in this figure, the proposed model closely captures the behavioral characteristics of the DAB converter circuit detailed model.
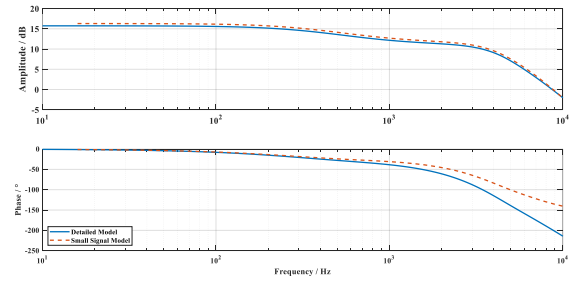

Fig. 7. Comparison detailed model and the proposed model for case 2.

C. Case 3: Duty Ratio Modulation for Secondary Bridge $(0 < D_2 < D_3 < 1 \cdot D_1 = 0)$

This situation is also similar to case 2, with the difference that there is an internal phase shift delay in the secondary bridge, and the diagonal switches in the primary bridge turn on and off without delay relative to each other. Bode diagram in this case is depicted in Fig. 8. As seen in this figure, the proposed model closely captures the behavioral characteristics of the DAB converter circuit detailed model.
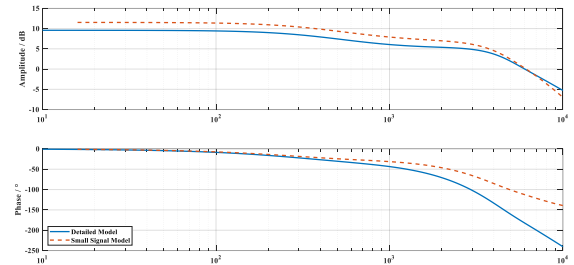

Fig. 8. Comparison detailed model and the proposed model for case 3.

D. Case 4: Duty Ratio Modulation for Both Bridges $(0 < D_1 < D_2 < D_3 < 1)$

This situation is similar to TPS modulation and represents a uniform modulation scheme which used in previous cases. In this state, there is a time delay for turning on and off the diagonal switches for both the primary and secondary bridges, and the secondary bridge has a phase shift delay relative to the primary bridge. Bode diagram in this case is depicted in Fig. 9. As seen in this figure, the proposed model closely captures the behavioral characteristics of the DAB converter circuit detailed model.
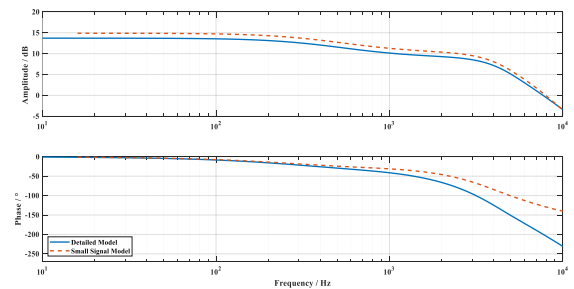

Fig. 9. Comparison detailed model and the proposed model for case 4.

As observed from the diagram results, the DAB converter exhibits the behavior of a first-order system, and the dynamics of the inductor current (i_L) do not affect the converter dynamic responses. This can be explained by the square nature of the primary and secondary transformer voltages at the switching

frequency (f_s), with their DC component equal to zero. In addition, the low-frequency components in the inductor current (i_L) cannot propagate to the converter's output because the current waveform is symmetrical and the average current over one cycle is zero. Therefore, disturbances in the inductor current due to changes in input voltage, output voltage, or phase-shift parameters do not affect the dynamics of the DAB converter, and the system will exhibit first-order behavior. Due to the modeling of nonlinear elements such as switches and transformers, some parasitic elements, including parasitic capacitance of the transformer and leakage inductance, are ignored for average modeling. The reason for the phase difference at higher frequencies in the Bode diagram is due to the removal of these parasitic elements, which have negligible values and, as observed, do not significantly affect the frequency response plot.

V. CONCLUSION

By simulating the nonlinear components included in the DAB converter's circuit, a reduced-order model is presented in this study. To make the suggested model more like actual circuits, it takes into account input and output filters in addition to any lossy components, such as transformer losses, conduction losses, and switching losses. By examining the small-signal model and obtaining the control transfer functions of the converter, frequency domain analysis of the DAB converter has been performed. Frequency analysis in 4 different cases shows that DAB act as a first-order system which means the dynamic of inductor current cannot propagate to the converter output due to the symmetry of the inductor current over one complete cycle. Comparison of simulation results demonstrates the satisfactory accuracy of the proposed model compared to the detailed model with nonlinear elements.

VI. REFERENCES

[1]   L. Li, G. Xu, D. Sha, Y. Liu, Y. Sun, and M. Su, "Review of Dual Active Bridge Converters with Topological Modifications," IEEE Transactions on Power Electronics, 2023.

[2]   M. A. Hannan, P. J. Ker, M. S. H. Lipu, Z. H. Choi, M. S. A. Rahman, K. M. Muttaqi, et al., "State of the art of solid-state transformers: Advanced topologies, implementation issues, recent progress and improvements," Ieee Access, vol. 8, pp. 19113-19132, 2020.

[3]   Y. Shi, R. Li, Y. Xue, and H. Li, "Optimized operation of current-fed dual active bridge DC–DC converter for PV applications," *IEEE Transactions on Industrial Electronics,* vol. 62, pp. 6986-6995, 2015.

[4]   S. P. Engel, N. Soltau, H. Stagge, and R. W. De Doncker, "Dynamic and balanced control of three-phase high-power dual-active bridge DC–DC converters in DC-grid applications," *IEEE Transactions on Power Electronics,* vol. 28, pp. 1880-1889, 2012.

[5]   D. A. Herrera-Jaramillo, D. Gonzalez Montoya, E. E. Henao-Bravo, C. A. Ramos-Paja, and A. J. Saavedra-Montes, "Systematic analysis of control techniques for the dual active bridge converter in photovoltaic applications," *International Journal of Circuit Theory and Applications,* vol. 49, pp. 3031-3052, 2021.

[6]   L. Xue, Z. Shen, D. Boroyevich, P. Mattavelli, and D. Diaz, "Dual active bridge-based battery charger for plug-in hybrid electric vehicle with charging current containing low frequency ripple," *IEEE Transactions on Power Electronics,* vol. 30, pp. 7299-7307, 2015.

[7]   F. Krismer and J. W. Kolar, "Efficiency-optimized high-current dual active bridge converter for automotive applications," *IEEE Transactions on Industrial Electronics,* vol. 59, pp. 2745-2760, 2011.

[8]   S. A. Assadi, H. Matsumoto, M. Moshirvaziri, M. Nasr, M. S. Zaman, and O. Trescases, "Active saturation mitigation in high-density dual-active-bridge DC–DC converter for on-board EV charger applications," *IEEE Transactions on Power Electronics,* vol. 35, pp. 4376-4387, 2019.

[9]   L. Jiang, Y. Sun, Y. Li, Z. Tang, F. Liu, Y. Yang, *et al.*, "Integrated Optimization of Dual-Active-Bridge DC-DC Converter with ZVS for Battery Charging Applications," *IEEE Journal of Emerging and Selected Topics in Power Electronics,* 2021.

[10]   B. Zhao, Q. Song, W. Liu, and Y. Sun, "Overview of dual-active-bridge isolated bidirectional DC–DC converter for high-frequency-link power-conversion system," *IEEE Transactions on power electronics,* vol. 29, pp. 4091-4106, 2013.

[11]   N. Hou and Y. W. Li, "Overview and comparison of modulation and control strategies for a nonresonant single-phase dual-active-bridge DC–DC converter," *IEEE Transactions on Power Electronics,* vol. 35, pp. 3148-3172, 2019.

[12]   K. Wu, C. W. de Silva, and W. G. Dunford, "Stability analysis of isolated bidirectional dual active full-bridge DC–DC converter with triple phase-shift control," *IEEE Transactions on Power Electronics,* vol. 27, pp. 2007-2017, 2011.

[13]   H. Bai, Z. Nie, and C. C. Mi, "Experimental comparison of traditional phase-shift, dual-phase-shift, and model-based control of isolated bidirectional DC–DC converters," *IEEE Transactions on Power Electronics,* vol. 25, pp. 1444-1449, 2009.

[14]   A. R. R. Alonso, J. Sebastian, D. G. Lamar, M. M. Hernando, and A. Vazquez, "An overall study of a Dual Active Bridge for bidirectional DC/DC conversion," in *2010 IEEE Energy Conversion Congress and Exposition*, 2010, pp. 1129-1135.

[15]   H. Bai, C. Mi, C. Wang, and S. Gargies, "The dynamic model and hybrid phase-shift control of a dual-active-bridge converter," in *2008 34th annual conference of IEEE industrial electronics* ,۲۰۰۸ ,pp. 2840-2845.

[16]   S. R. Sanders, J. M. Noworolski, X. Z. Liu, and G. C. Verghese, "Generalized averaging method for power conversion circuits," *IEEE Transactions on power Electronics,* vol. 6, pp. 251-259, 1991.

[17]   H. Qin and J. W. Kimball, "Generalized average modeling of dual active bridge DC–DC converter," *IEEE Transactions on power electronics,* vol. 27, pp. 2078-2084, 2011.

[18]   C. Zhao, S. D. Round, and J. W. Kolar, "Full-order averaging modelling of zero-voltage-switching phase-shift bidirectional DC–DC converters," *IET Power Electronics,* vol. 3, pp. 400-410, 2010.

[19]   L. Shi, W. Lei, Z. Li, J. Huang, Y. Cui, and Y. Wang, "Bilinear discrete-time modeling and stability analysis of the digitally controlled dual active bridge converter," *IEEE Transactions on Power Electronics,* vol. 32, pp. 8787-8799, 2016.

[20]   F. Krismer and J. W. Kolar, "Accurate small-signal model for the digital control of an automotive bidirectional dual active bridge," *IEEE transactions on power electronics,* vol. 24 ,pp. 2756-2768, 2009.

[21]   G. C. Verghese, M. E. Elbuluk, and J. G. Kassakian, "A general approach to sampled-data modeling for power electronic circuits," *IEEE Transactions on Power Electronics,* pp. 76-89, 1986.

[22]   P. Wang, C. Liu, and L. Guo, "Modeling and simulation of full-bridge series resonant converter based on generalized state space averaging," *Applied Mechanics and Materials,* vol. 347, pp. 1828-1832, 2013.

[23]   S. Shao, L. Chen, Z. Shan, F. Gao, H. Chen, D. Sha, *et al.*, "Modeling and advanced control of dual-active-bridge DC–DC converters: A review," *IEEE Transactions on Power Electronics,* vol. 37, pp. 1524-1547, 2021.

[24]   J. He, Y. Chen, J. Lin, J. Chen, L. Cheng, and Y. Wang, "Review of Modeling, Modulation, and Control Strategies for the Dual-Active-Bridge DC/DC Converter," *Energies,* vol. 16, p. 6646, 2023.

[25]   D. Costinett, "Reduced order discrete time modeling of ZVS transition dynamics in the dual active bridge converter," in *2015 IEEE Applied Power Electronics Conference and Exposition (APEC)*, 2015, pp. 365-370.

[26]   B. Farhangi and H. A. Toliyat, "Piecewise linear model for snubberless dual active bridge commutation," *IEEE Transactions on Industry Applications,* vol. 51, pp. 4072-4078, 2015.

[27]   H. Bai, Z. Nie, and C. C. Mi, "Experimental comparison of traditional phase-shift, dual-phase-shift, and model-based control of isolated bidirectional DC–DC converters," *IEEE Transactions on Power Electronics,* vol. 25, pp. 1444-1449, 2010.

[28]   X. Li and Y.-F. Li, "An optimized phase-shift modulation for fast transient response in a dual-active-bridge converter," *IEEE Transactions on Power Electronics,* vol. 29, pp. 2661-2665, 2013.

[29]   R. W. Erickson and D. Maksimovic, *Fundamentals of power electronics*: Springer Science & Business Media, 2007.

[30]   K. Zhang, Z. Shan, and J. Jatskevich, "Large-and small-signal average-value modeling of dual-active-bridge DC–DC converter considering power losses," *IEEE Transactions on Power Electronics,* vol. 32, pp. 1964-1974, 2016.

[31] P. Wang, X. Chen, C. Tong, P. Jia, and C. Wen, "Large-and small-signal average-value modeling of dual-active-bridge DC–DC converter with triple-phase-shift control," *IEEE Transactions on Power Electronics,* vol. 36, pp. 9237-9250, 2021.

[32] D. Graovac, M. Purschel, and A. Kiep, "MOSFET power losses calculation using the data-sheet parameters," *Infineon application note,* vol. 1, pp. 1-23, 2006.